Title

Interaction of the Influenza A Virus NS1 Protein with the 5′-m7G-mRNA·eIF4E·eIF4G1 Complex

Journal

Biochemistry, 61(14)

ISSN

0006-2960

Authors

Cruz, Alejandro

Joseph, Simpson

Publication Date

2022-07-19

DOI

10.1021/acs.biochem.2c00019

Biochemistry

pubs.acs.org/biochemistry Article

Interaction of the Influenza A Virus NS1 Protein with the 5′-m7G-mRNA·eIF4E·eIF4G1 Complex

Alejandro Cruz and Simpson Joseph*

Cite This: *Biochemistry* 2022, 61, 1485−1494 Read Online

ACCESS | Metrics & More | Article Recommendations | Supporting Information

ABSTRACT: The influenza A virus (IAV) is responsible for seasonal epidemics that result in hundreds of thousands of deaths worldwide annually. The non-structural protein 1 (NS1) of the IAV inflicts various antagonistic processes on the host during infection. These processes include inhibition of the host interferon system, inhibition of the apoptotic response, and enhancement of viral mRNA translation, all of which contribute to the overall virulence of the IAV. Although the mechanism by which NS1 stimulates translation is unknown, NS1 has been shown to bind both poly-A binding Protein 1 and eukaryotic initiation factor 4 gamma 1 (eIF4G1), two proteins necessary for cap-dependent translation. We directly analyzed the interaction between NS1 and eIF4G1 within the context of the 5′-m^{7}G-mRNA·eIF4E·eIF4G1 complex. Interestingly, our studies show that NS1 can bind this complex in the presence or absence of 5′-m^{7}G-mRNA. Additionally, we were interested in investigating whether NS1 interacts with eIF4E directly. Our results indicate that NS1 can bind to eIF4E only in the absence of 5′-m^{7}G-mRNA. Considering previous data, we propose that NS1 stimulates translation by binding to eIF4G1 and recruiting the 43S pre-translation initiation complex to the mRNA.

INTRODUCTION

Between 2010 through 2015, the seasonal influenza A virus (IAV) was responsible for 9 million to 36 million influenza-associated illnesses in the United States alone.[1] In 2003, the direct medical cost in the United States due to seasonal IAV epidemics was estimated to be $10 billion, while the total economic burden was estimated at $87 billion.[2] Human IAV infection occurs in the upper and lower respiratory tract and is characterized by, but is not limited to, fever, cough, headache, and inflammation of the upper respiratory tree and trachea.[3]

IAVs are members of the *Orthomyxoviridae* family, whose viral genome contains eight single-stranded, negative-sense RNA segments, which encode 10 to 12 viral proteins.[4−7] Among the IAV proteins, the non-structural protein 1 (NS1) is the main antagonist of the host's innate immunity. NS1 is responsible for various processes that contribute to effective viral replication and virulence, including suppression of host immune and apoptotic responses, enhancement of viral mRNA translation, and post-transcriptional blocking of processing, and nuclear exporting of cellular mRNAs.[8,9]

The NS1 protein is 26 kDa and is traditionally divided into four distinct regions, the N-terminal RNA-binding domain (RBD) (amino acids 1 through 73), the linker region (amino acids 73 through 88), followed by the effector domain (ED) (amino acids 88 through 202) and the C-terminal tail (amino acids 202 through 237).[8,10,11] Excluding the high sequence variation in the C-terminal tail and linker region, the domains are highly conserved for NS1 proteins from various IAVs, highlighting the utility of these domains.[12]

Although NS1 is known to interact with many host proteins, we were interested in better characterizing the interaction between NS1 and eukaryotic translation initiation factor 4 gamma 1 (eIF4G1).[8] eIF4G1 is a crucial component of the translation initiation factor complex, serving as a scaffolding protein that binds other initiation factors, stimulating their activity and recruiting ribosomes to the mRNA.[13−15] The NS1−eIF4G1 interaction was mapped to amino acids 157 through 550 on eIF4G1 and amino acids 82 through 113 on NS1 (Figure 1A).[16] Although the reason for NS1's binding to eIF4G1 is not yet understood, we sought to study this interaction directly and in the context of eIF4E and 5′-m^{7}G-mRNA as all three biomolecules form a single complex during translation initiation.[17,18] In addition to eIF4G1, we were interested in investigating the possibility of NS1 interacting with eIF4E independently of eIF4G1. Using a combination of

Received: January 11, 2022
Revised: June 8, 2022
Published: July 7, 2022

https://doi.org/10.1021/acs.biochem.2c00019
Biochemistry 2022, 61, 1485−1494

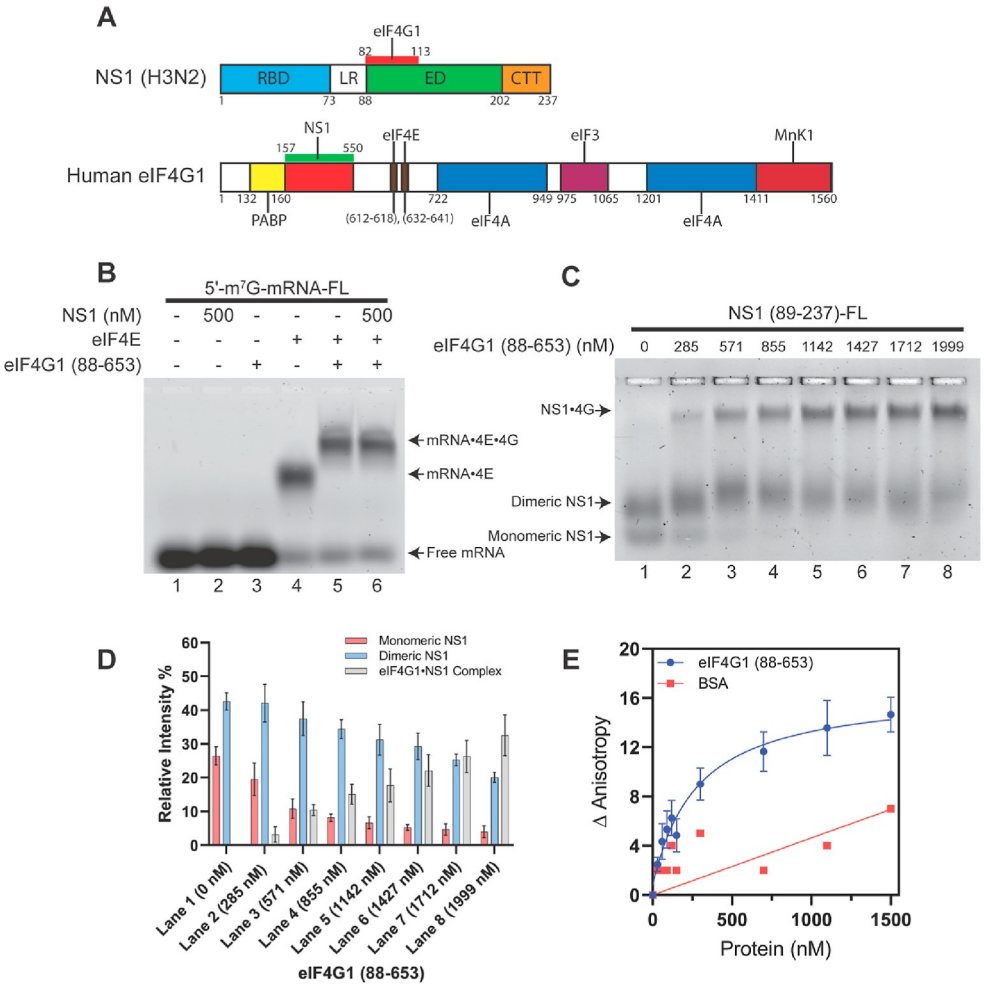

Figure 1. The ED of NS1 is sufficient for binding to human eIF4G1. (A) Cartoon diagram depicting the functional domains in NS1 and eIF4G1.[11,16,17,27] The red line indicates the eIF4G1-binding region in NS1. Labels: LR, linker region; CTT, C-terminal tail. The red box indicates the NS1-binding region in eIF4G1. The other protein-binding regions in eIF4G1 are also shown. (B) Representative EMSA showing that wildtype H5N1 NS1 does not cause an apparent shift of the 5′-m^{7}G-mRNA·eIF4E·eIF4G1 complex. The absence and presence of the different proteins are indicated by the minus and plus signs, respectively, above the lanes. The concentrations are 5′-m^{7}G-mRNA-FL = 50 nM, NS1 = 500 nM, eIF4E = 500 nM, and eIF4G1 (88−653) = 500 nM. (C) Representative EMSA showing that the fluorescein-labeled H3N2 NS1 (89−237) interacts directly with eIF4G1 (88−653). The concentration of NS1 (89−237)-FL was set to 75 nM, while the eIF4G1 (88−653) concentration was increased from 0 to 1999 nM in 285 nM steps. (D) Quantification of the changes in band intensities in the EMSA caused by the titration of eIF4G1 (88−653). Error bars show the standard deviations from three independent experiments. (E) Graph showing the increase in fluorescence anisotropy of fluorescently labeled NS1 (89−237) caused by the addition of eIF4G1 (88−653). The change in fluorescence anisotropy caused by BSA was also measured to test for non-specific protein−protein interactions. Error bars display the standard deviations from four independent experiments.

fluorescence anisotropy and native electrophoretic assays, we detail the interactions between NS1, eIF4E, eIF4G1, and 5′-m^{7}G-mRNA. Our results show that NS1 can bind eIF4E and eIF4G1 separately and the eIF4G1·eIF4E complex. Interestingly, we found that the NS1·eIF4E complex is outcompeted by forming the higher-affinity 5′-m^{7}G-mRNA·eIF4E complex. Nevertheless, NS1 can bind to the 5′-m^{7}G-mRNA·eIF4E·eIF4G1 complex by directly interacting with eIF4G1. The interaction of NS1 with eIF4G1 may be necessary for translation stimulation.

MATERIALS AND METHODS

Purification of Recombinant NS1 from the H3N2 and H5N1 Strains. The NS1 coding sequences from the H3N2 influenza virus and the H5N1 influenza virus were independently subcloned into the pETHSUL vector.[19] The NS1 (89−237) construct was created by deleting the first 88 amino acids and the 5′-SUMO tag from the wildtype H3N2 NS1 sequence by PCR. The vectors encoding the constructs were then transformed into *Escherichia coli* BL21 (DE3) cells. For expression, 2 L of bacterial cells were grown at 37 °C in Luria−Bertani (LB) broth supplemented with ampicillin until the OD_{600} reached a value between 0.6 and 0.8. At this point, isopropyl *β*-D-1-thiogalactopyranoside (IPTG) was added to a final concentration of 1 mM, and the cells were incubated for an additional 3 h. Following the induction period, the cells were harvested, flash-frozen, and stored at −80 °C.

Cells expressing NS1 (89-237) were resuspended in 50 mL of lysis buffer [50 mM HEPES (pH 7.5), 300 mM NaCl, 0.5 mM EDTA, 15 mM imidazole, 5% glycerol, 0.1% Triton X-100, 8 mM dithiothreitol (DTT), and 1 mM phenylmethylsulfonyl fluoride (PMSF)] and then sonicated to lyse. The cell lysate was clarified by centrifugation at 20,000*g* for 45 min at 4 °C. The supernatant was incubated with 1 mL of equilibrated Ni-NTA resin for 2 h. The cell-slurry mixture was

https://doi.org/10.1021/acs.biochem.2c00019
Biochemistry 2022, 61, 1485−1494

poured over a column and washed with 50 column volumes (CVs) of wash buffer A [50 mM HEPES (pH 7.5), 300 mM NaCl, 0.5 mM EDTA, 40 mM imidazole, 5% glycerol, 8 mM DTT, and 1 mg/mL of heparin sodium salt] and then with 25 CVs of wash buffer B [50 mM HEPES (pH 7.5), 1 M NaCl, 0.5 mM EDTA, 40 mM imidazole, 5% glycerol, and 8 mM DTT]. Finally, the beads were washed with 25 CVs of wash buffer C [50 mM HEPES (pH 7.5), 300 mM NaCl, 0.5 mM EDTA, 5% glycerol, and 8 mM DTT]. The protein was eluted with an elution buffer [50 mM HEPES (pH 7.5), 300 mM NaCl, 0.5 mM EDTA, 5% glycerol, 8 mM DTT, and 250 mM imidazole]. Eluates were concentrated, filtered, and further purified with a Superdex 16/600 200 size exclusion column with a running buffer consisting of storage buffer A [50 mM HEPES (pH 7.5), 300 mM NaCl, 10% glycerol, and 1 mM tris(2-carboxyethyl)phosphine (TCEP-HCl)], using a flow rate of 1 mL per minute. The elution peaks were analyzed by SDS−PAGE and fractions free of nucleic acid (determined by measuring the 260/280 ratio with a Spectrophotometer NanoDrop 2000C instrument) and protein contaminations were concentrated, aliquoted, and flash-frozen. All protein constructs were stored at −80 °C. The concentrations of the protein aliquots were determined by the Bradford assay (Bio-Rad).

The purification of the wildtype H5N1 was performed as previously described.[20] The protein concentration was measured by the Bradford assay (Bio-Rad). The purified protein was aliquoted, flash-frozen, and stored at −80 °C.

Purification of Recombinant eIF4G1. A codon-optimized DNA coding for amino acids 88 through 653 of the human eIF4G1 was purchased for expression in an *E. coli* system (GENEWIZ). The sequence was subcloned into the pTXB1 vector (New England Biolabs) with the addition of a threonine following the coding sequence to enhance intein cleavage. The plasmid was then transformed into BL21(DE3) Star *E. coli* cells. For expression, 2 L of bacterial cells were grown at 37 °C in LB broth supplemented with ampicillin until the OD_{600} reached a value between 0.6 and 0.8. Subsequently, the cells were induced with 0.4 mM IPTG and allowed a 2.5 h induction period at 30 °C. Following induction, the cells were harvested, flash-frozen, and stored at −80 °C.

The eIF4G1-containing cells were resuspended in 50 mL of lysis buffer [20 mM HEPES (pH 8.2), 1 M KCl, 20% glycerol, 1 mM EDTA, and 1 mM PMSF] and then sonicated to lyse. The cell lysate was clarified by centrifugation at 20,000*g* for 45 min at 4 °C. The supernatant was incubated with 7 mL of equilibrated chitin resin for 2 h at 4 °C. Following the incubation, the beads were poured over a column and washed with 8 CVs of buffer A [20 mM HEPES (pH 7.5), 100 mM KCl, 10% glycerol, 0.1 mM EDTA, 0.5 mM TCEP, and 1 mg/mL of heparin sodium salt] and then 20 CVs of lysis buffer (without the 1 mM PMSF), followed by 7 CVs of storage buffer A [20 mM HEPES (pH 7.5), 100 mM KCl, 10% glycerol, 0.1 mM EDTA, and 0.5 mM TCEP]. To catalyze the intein cleavage reaction, 4 CVs of cleavage buffer [20 mM HEPES (pH 7.5), 100 mM KCl, 10% glycerol, 0.1 mM EDTA, 0.5 mM TCEP, and 50 mM DTT] was added to the resin and then allowed to tumble overnight at room temperature. Following the overnight incubation, the supernatant was concentrated, filtered, and loaded onto a Superdex 75 16/600 size exclusion column with a running buffer consisting of storage buffer A using a flow rate of 1 mL per minute. Elution peaks were analyzed by SDS−PAGE, and fractions free of nucleic acid (determined by measuring the 260/280 ratio with a Spectrophotometer NanoDrop 2000C instrument) and protein contamination were concentrated and aliquoted. The concentrations of the protein aliquots were then determined by the Bradford assay. Finally, the aliquots were flash-frozen and stored at −80 °C.

Purification of Recombinant eIF4E. The plasmid containing the coding sequence for human eIF4E was purchased from Addgene and subcloned into the expression vector pMCSG26. The plasmid was then transformed into the *E. coli* Rosetta 2 (DE3) pLysS strain. For expression, 2 L of bacterial cells were grown at 37 °C in LB broth supplemented with ampicillin and chloramphenicol until the OD_{600} reached a value between 0.6 and 0.8. The cells were induced with 0.2 mM IPTG and allowed a 16 h induction period at 14 °C. Following the induction period, the cells were harvested, flash-frozen, and stored at −80 °C.

eIF4E-containing cells were resuspended in 200 mL of lysis buffer [100 mM Tris−HCl (pH 8.0), 100 mM KCl, 10% glycerol, 5 mM imidazole, 5 mM β-mercaptoethanol, and 1 mM PMSF]. The cells were lysed by the French press and clarified by centrifugation at 20,000*g* for 45 min at 4 °C. The supernatant was incubated with 1.5 mL of equilibrated Ni-NTA resin for 2 h. The resin was poured over a column and washed with 30 CVs of wash buffer A [100 mM Tris−HCl (pH 8.0), 100 mM KCl, 10% glycerol, 5 mM imidazole, 5 mM β-mercaptoethanol, and 1 mg/mL heparin sodium salt] and then 30 CVs of wash buffer B [100 mM Tris−HCl (pH 8.0), 1 M KCl, 10% glycerol, and 5 mM β-mercaptoethanol], followed by 30 CVs of wash buffer C [100 mM Tris−HCl (pH 8.0), 100 mM KCl, 10% glycerol, and 20 mM imidazole]. The protein was eluted by adding 30 CVs of elution buffer [20 mM Tris−HCl (pH 8.0), 100 mM KCl, 10% glycerol, 5 mM β-mercaptoethanol, and 250 mM imidazole] and allowed to incubate at room temperature for 15 min. The supernatant was concentrated, filtered, and loaded onto a Superdex 75 16/600 size exclusion column with running buffer A [20 mM Tris−HCl (pH 8.0), 100 mM NaCl, and 10% glycerol]. Elution peaks were analyzed by SDS−PAGE, and fractions containing the protein of interest were collected, concentrated, and then loaded onto a HiTrap Q anion exchange column. The Hitrap Q column utilized two buffers for the NaCl gradient, a low NaCl buffer [20 mM Tris−HCl (pH 8.0), 10% glycerol, and 100 mM NaCl] and a high NaCl buffer [20 mM Tris−HCl (pH 8.0), 10% glycerol, and 1 M NaCl]. The elution peaks were analyzed through SDS−PAGE and fractions free of nucleic acid (determined by measuring the 260/280 ratio with a Spectrophotometer NanoDrop 2000C instrument) and protein contamination were concentrated and aliquoted. The concentrations of the protein aliquots were determined by the Bradford assay and then stored at −80 °C.

mRNA for the Electrophoretic Mobility Shift Assay. The mRNA (5′-GGGUGACAGUCCUGUUU-3′) was synthesized by T7 RNA polymerase transcription in vitro and purified by denaturing urea-PAGE, chloroform extraction, and ethanol precipitation. The mRNA was resuspended in water, and the concentration was determined by measuring the absorbance at 260 nm and then aliquoted and stored at −80 °C. The 3′ end of the mRNA was fluorescently labeled with either fluorescein 5-thiosemicarbazide (Invitrogen) or CF-555 hydrazide (Biotium) by first oxidizing the 3′ end with a solution consisting of 100 mM sodium acetate (pH 5.2) and 100 μM potassium periodate for 90 min at room temperature.

https://doi.org/10.1021/acs.biochem.2c00019
Biochemistry 2022, 61, 1485−1494

Then, the oxidized mRNA was purified from the oxidizing solution using a Monarch RNA Clean-up Kit (New England BioLabs). The oxidized mRNA was then incubated with either Fluorescein 5-thiosemicarbazide or CF-555 hydrazide overnight at 4 °C. A 7-methylguanylate cap was added to the 5′ end of mRNA using the vaccinia capping system.[21]

Fluorescence Labeling of the NS1 Construct. The NS1 (89−237) protein was labeled with *N*-(5-fluoresceinyl) maleimide (Sigma-Aldrich) at the cysteine at amino acid position 116. The labeling reaction was performed according to the manufacturer's specifications, and the unreacted dye was removed by multiple Bio-Spin 6 columns (Bio-Rad). To ensure that no unreacted dye remained, the labeled protein was analyzed by SDS−PAGE and imaged using a FLA9500 Typhoon instrument using the Cy2 excitation laser. The labeled protein was then concentrated, and the concentration was determined by measuring the A280 with a Spectrophotometer NanoDrop 2000C instrument. The labeled protein was then aliquoted, flash-frozen, and stored at −80 °C.

Electrophoretic Mobility Shift Assay. We modified a previously described procedure to analyze the various biomolecular interactions through native gel electrophoresis.[22] The electrophoretic mobility shift assays (EMSAs) were conducted by incubating different combinations of mRNA and protein with one or two biomolecules labeled with their respective fluorophores in anisotropy buffer [50 mM HEPES (pH 7.4), 150 mM NaCl, 5% Glycerol, and 0.01% Tween 20] (with 50 ng/μL *E. coli* total tRNA if RNA binding is involved) to a final volume of 20 μL at room temperature for 1 h. Unless otherwise stated, the concentration of the fluorescently labeled 5′-m^{7}G-mRNA (either fluorescein or CF-555) was kept at 50 nM, whereas the concentration of the fluorescein-labeled NS1 (89-237) (H3N2) mutant was kept at 75 nM, and the concentrations of both eIF4G1 and eIF4E were kept at 500 nM. Following incubation, 1 μL of a pre-chilled 50% glycerol and xylene cyanol mixture (xylene cyanol was excluded if CF-555 was included) was added to the solutions. The complexes were separated from unbound species on a non-denaturing gel made from a 0.7% SEAKEM GTG agarose solution and 0.5× TBE buffer. The EMSA was performed at 4 °C in 0.5× TBE running buffer and held to a constant voltage of 66 V for 1.5 h. The gels were visualized by scanning with either a FLA9500 Typhoon or an Amersham Typhoon instrument, using Cy2 or Cy3 excitation. The analysis and quantification of the relative intensity percentage of the various EMSAs were determined using ImageJ.[23]

Fluorescence Anisotropy. Fluorescence anisotropy experiments were conducted using a fixed concentration of fluorescein-labeled mutant NS1 (H3N2) and an increasing concentration of the other protein in the anisotropy buffer [50 mM HEPES (pH 7.4), 150 mM NaCl, 5% Glycerol, and 0.01% Tween 20]. The labeled NS1 (89-237) was fixed at a concentration of 20 nM while either eIF4G1 or eIF4E were added in a concentration ranging from 0 to 1500 nM or 0 to 850 nM, respectively. Samples were incubated at room temperature for 1 h in a 384-well plate and then measured using a Tecan Spark instrument. The excitation was set at 470 nm, and polarized emission was measured at 520 nm. A 10 nm band slit was used for both the excitation and emission. The *G*-factor was previously determined using a control sample with fluorescein-labeled mRNA. The anisotropy values were subtracted from the baseline value, plotted, and fit to the following quadratic equation to determine the K_D value as described previously[24]

$$\frac{[P + FL]}{[FL]} = \frac{[[P] + [FL] + K_D - \sqrt{([P] + [FL] + K_D)^2 - 4[P][FL]}\,]}{(2[P])}$$

where [P + FL]/[FL] is the anisotropy value, [FL] is the fluorescently labeled species, and [P] is the protein concentration. GraphPad Prism (GraphPad Software Inc.) was used to determine the curve fit. All experiments were performed at least three times with different protein batches to confirm the reproducibility of the results.

RESULTS

NS1 Binds to Human eIF4G1. Previous studies have shown that amino acids 81 through 113 of NS1 are sufficient for in vivo and in vitro binding to eIF4G1.[16] We investigated whether the interaction between eIF4G1 (88−653) and full-length H5N1 NS1 affected the formation of the 5′-m^{7}G-mRNA-bound eIF4E·eIF4G1 complex using an EMSA. The EMSA showed that we could assemble the 5′-m^{7}G-mRNA·eIF4E·eIF4G1 complex; however, we did not observe any change to this complex in the presence of NS1 (Figure 1B). Since our results were inconclusive, we decided to label NS1 with a fluorescent dye to directly track its location in the presence of the 5′-m^{7}G-mRNA·eIF4E·eIF4G1 complex. We used a fragment of NS1, NS1 (89−237), rather than the full-length NS1 because it is easier to prepare in large amounts and remains stable during the conjugation reaction with fluorescent dyes. Additionally, we can use fluorescence anisotropy to quantitatively determine binding affinities with other proteins because of the smaller size of the NS1 (89−237) fragment. NS1 (89−237) was labeled with fluorescein, and binding to eIF4G1 was first analyzed by EMSA. NS1 (89−237) by itself migrated as two bands in the native gel, which may correspond to the monomer and dimer of the ED, as reported previously.[25,26] The addition of an increasing concentration of eIF4G1 resulted in the appearance of the NS1·eIF4G1 band and the simultaneous disappearance of the NS1 (89−237) bands (Figure 1C). Interestingly, we noticed that the monomer band was the first to disappear, while the dimers' intensity was slow to fade (Figure 1D). To ensure that the formation of the NS1·eIF4G1 band was not a result of non-specific interactions, a control EMSA was performed using bovine serum albumin (BSA) added in identical concentrations to FL-labeled NS1 (89−237); no new band formation was observed (Figure S1A). Next, we used a fluorescence polarization assay to monitor the change in anisotropy of FL-labeled NS1 (89−237) in the presence of an increasing concentration of eIF4G1 (Figure 1E). The anisotropic data were analyzed by non-linear regression to attain an equilibrium dissociation constant (K_D) of 264 ± 63 nM. As a control, BSA was added in identical eIF4G1 concentrations, and a non-specific linear change in anisotropy was observed (Figure 1E). Our results show that NS1 binds with specificity to eIF4G1.

NS1 Binds to Human eIF4E. Previous studies have explored the importance of eIF4E in the influenza viral life cycle.[28−30] For example, a study found that influenza virus infection proceeds without hindrance in various conditions where eIF4E is functionally impaired.[28] Additionally, the same

https://doi.org/10.1021/acs.biochem.2c00019
Biochemistry 2022, 61, 1485−1494

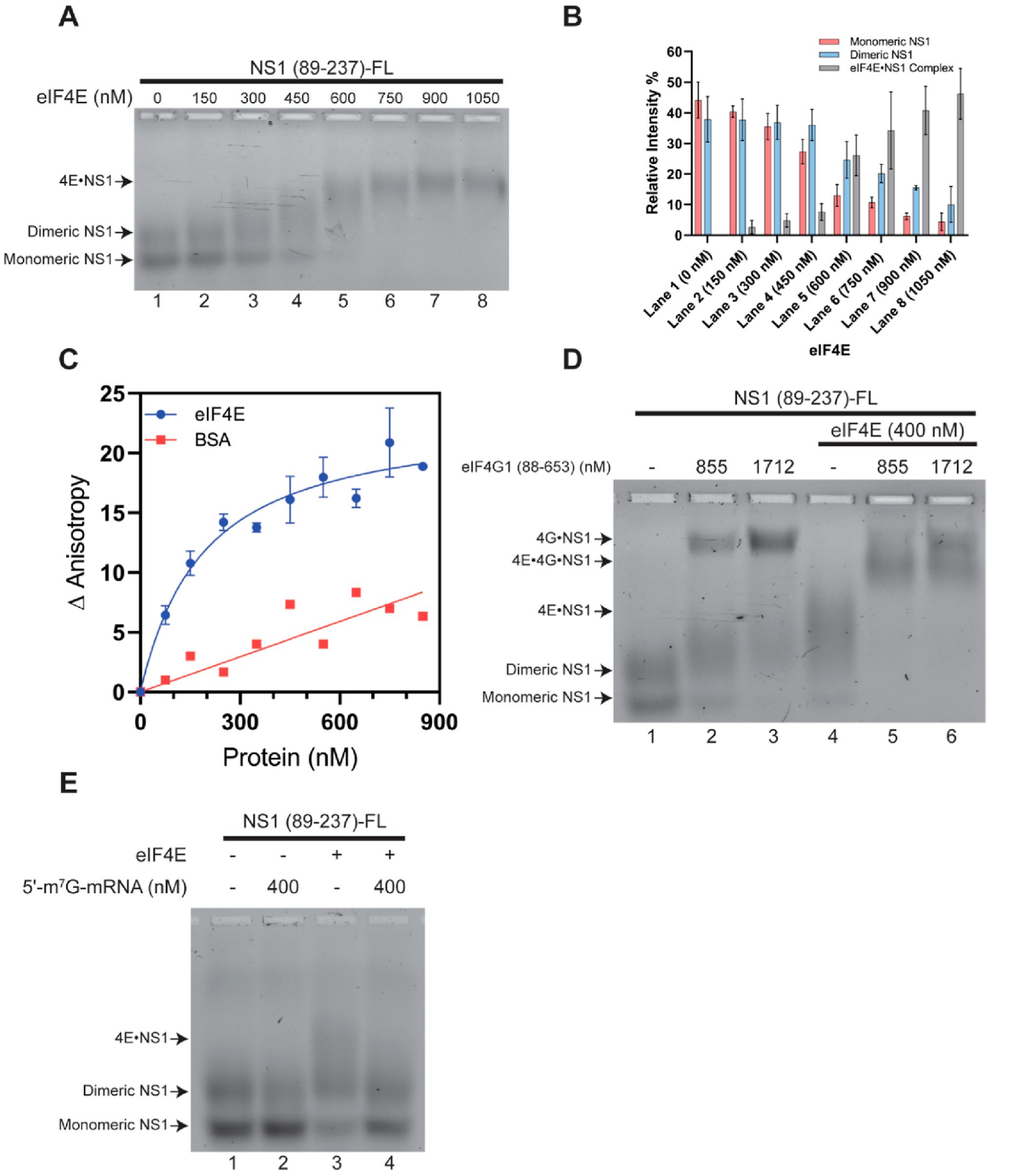

Figure 2. The ED of NS1 binds to human eIF4E in the absence of 5′-m^{7}G-mRNA. (A) Representative EMSA showing that the fluorescein-labeled NS1 (89−237) interacts directly with eIF4E. The concentration of NS1 (89−237)-FL was set to 75 nM, while the eIF4E concentration was increased from 0 to 1050 nM in 150 nM steps. (B) Quantification of the changes in band intensities in the EMSA caused by the titration of eIF4E. The error bars depict the standard deviations from three independent experiments. (C) Graph showing the increase in fluorescence anisotropy of fluorescently labeled NS1 (89−237) caused by the addition of eIF4E. The change in fluorescence anisotropy caused by BSA was also measured to test for non-specific protein−protein interactions. The error bars show the standard deviations from three independent experiments. (D) Representative EMSA showing the formation of the eIF4E·eIF4G1·NS1 complex. The concentrations are NS1 (89−237)-FL = 75 nM, eIF4E = 400 nM, and eIF4G1 (88−653) = 855 or 1712 nM. (E) Representative EMSA showing that the addition of 5′-m^{7}G-mRNA disrupts the eIF4E·NS1 (89−237) complex. The concentrations are NS1 (89−237)-FL = 75 nM, eIF4E = 400 nM, and 5′-m^{7}G-mRNA = 400 nM.

https://doi.org/10.1021/acs.biochem.2c00019
Biochemistry 2022, 61, 1485−1494

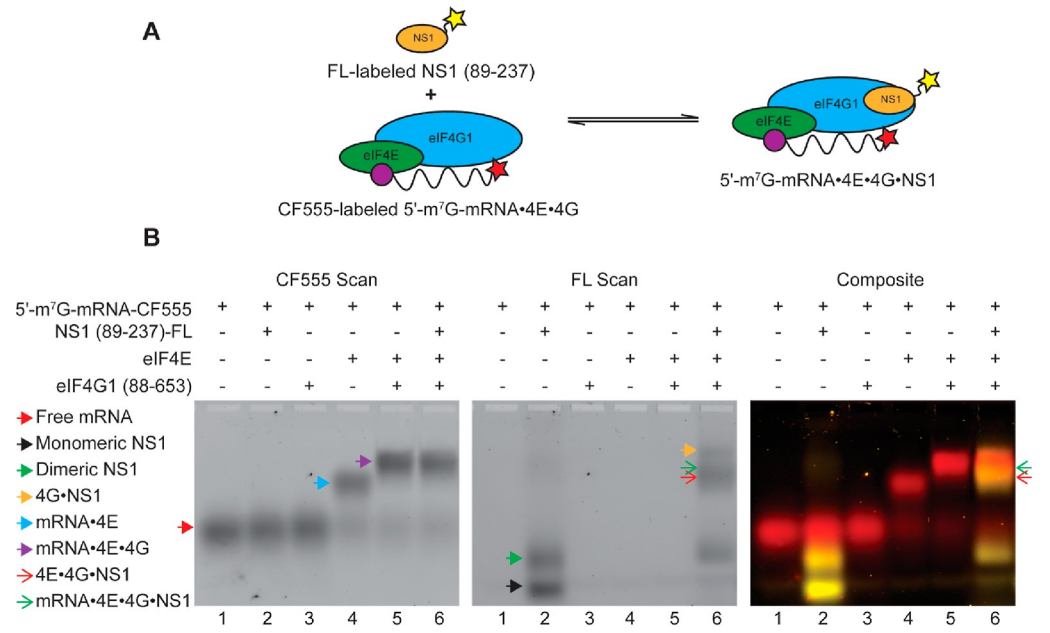

Figure 3. NS1 (89−237) colocalizes with the 5′-m^{7}G-mRNA·eIF4E·eIF4G1 (88−653) complex. (A) Cartoon depiction of the fluorescein-labeled NS1 (89−237) binding to the 5′-m^{7}G-mRNA-CF555·eIF4E·eIF4G1 complex. (B) Representative EMSA showing the formation of the 5′-m^{7}G-mRNA-CF555·eIF4E·eIF4G1 (88−653) complex detected by scanning for CF555 fluorescence emission (left panel), fluorescein emission (middle panel), and an overlay of both scans with CF555 emission shown in red and fluorescein emission shown in yellow (right panel). The plus and minus signs indicate the presence and absence of the indicated biomolecule. The colored arrowheads indicate each designated complex or unbound fluorophore-labeled protein or mRNA.

group that first reported the NS1 and eIF4G1 interaction reported that eIF4E could not bind NS1.[16] However, the binding studies were performed with the rabbit reticulocyte lysate in vitro translation system, in which eIF4E may have been pre-bound to 5′-m^{7}G-mRNA. Therefore, we investigated whether NS1 could bind to eIF4E that is not attached to 5′-m^{7}G-mRNA. We used an EMSA to monitor the binding of NS1 (89−237) to human eIF4E. NS1 (89−237) labeled with fluorescein was incubated with an increasing concentration of eIF4E and analyzed by a native gel. We observed the appearance of a new band representing the NS1·eIF4E complex (Figure 2A). Interestingly, unlike eIF4G1, there was no residual dimer band at high concentrations of eIF4E, and both the monomer and dimer band intensities decreased at similar rates (Figure 2B). Next, we used a fluorescence anisotropy assay to determine the equilibrium dissociation constant (K_D) for NS1 (89−237) binding to eIF4E (Figure 2C). The K_D for NS1 binding to eIF4E interaction was determined to be 177 ± 39 nM, which is comparable to the measured K_D for the NS1 and eIF4G1 interaction. To validate our results, we performed control experiments with increasing concentrations of BSA added to FL-labeled NS1 and observed a non-specific linear anisotropy change. Thus, we discovered that NS1 binds to eIF4E in the absence of mRNA. The ED of the NS1 protein is highly conserved throughout multiple influenza viruses, suggesting that the interaction with eIF4E may occur for other influenza A strains.[12,26]

Interaction of NS1 with the 5′-m^{7}G-mRNA·eIF4E·eIF4G1 complex. Since our studies showed that NS1 could bind to eIF4G1 and eIF4E separately, we decided to investigate whether NS1 would bind to the eIF4E·eIF4G1 complex. We performed an EMSA with FL-labeled NS1 (89−237) in the presence of two concentrations of eIF4G1 (855 and 1712 nM), both with and without eIF4E. We observed a new band when both eIF4E and eIF4G1 were present, indicating the formation of an NS1·eIF4E·eIF4G1 complex located below the NS1·eIF4G1 complex (Figure 2D, lane 5). Thus, our studies showed that NS1 could bind to eIF4E and eIF4G1 separately and the eIF4E·eIF4G1 complex. In the presence of 1712 nM eIF4G1, NS1 (89−237) predominantly forms the NS1·eIF4G1 complex rather than the NS1·eIF4E·eIF4G1 ternary complex because eIF4G1 is present in 3.2-fold molar excess over eIF4E, and NS1 (89−237) has similar binding affinities for eIF4E and eIF4G1.

To determine whether NS1 could bind to the 5′-m^{7}G-mRNA·eIF4E complex, we performed an EMSA with NS1 (89−237)-FL and eIF4E in the presence of excess 5′-m^{7}G-mRNA. NS1 (89−237)-FL in the absence and presence of 5′-m^{7}G-mRNA showed an identical band pattern, indicating that it does not bind to 5′-m^{7}G-mRNA (Figure 2E, compare lanes 1 and 2). As shown above, NS1 (89−237)-FL binds to eIF4E (Figure 2E, lane 3 shows a smear above the NS1 dimer band corresponding to the NS1·eIF4E complex). Interestingly, in the presence of excess 5′-m^{7}G-mRNA, NS1 (89−237) no longer binds to eIF4E (Figure 2E, lane 4 shows the monomer and dimer bands of NS1 as seen in the control lane 1). However, in the presence of the excess m^{7}G(5′)ppp(5′)G cap analogue, the binding of NS1 (89−237) to eIF4E was not inhibited (Figure S1C). This difference in results suggests that the ribonucleotides following the 5′-m^{7}G cap analogue may sterically hinder NS1's ability to bind eIF4E. We theorize that NS1 may bind near the cap-binding pocket of eIF4E but not directly to the cap-binding site. We attempted to demonstrate the inverse, where excess NS1 was added to disrupt the binding of eIF4E to capped RNA but were unsuccessful (Figure S1B). We reason that NS1's inability to disrupt the 5′-m^{7}G-RNA·eIF4E complex is because eIF4E has a higher affinity for 5′-m^{7}G-mRNA (K_D = 60 nM, which is significantly

https://doi.org/10.1021/acs.biochem.2c00019
Biochemistry 2022, 61, 1485−1494

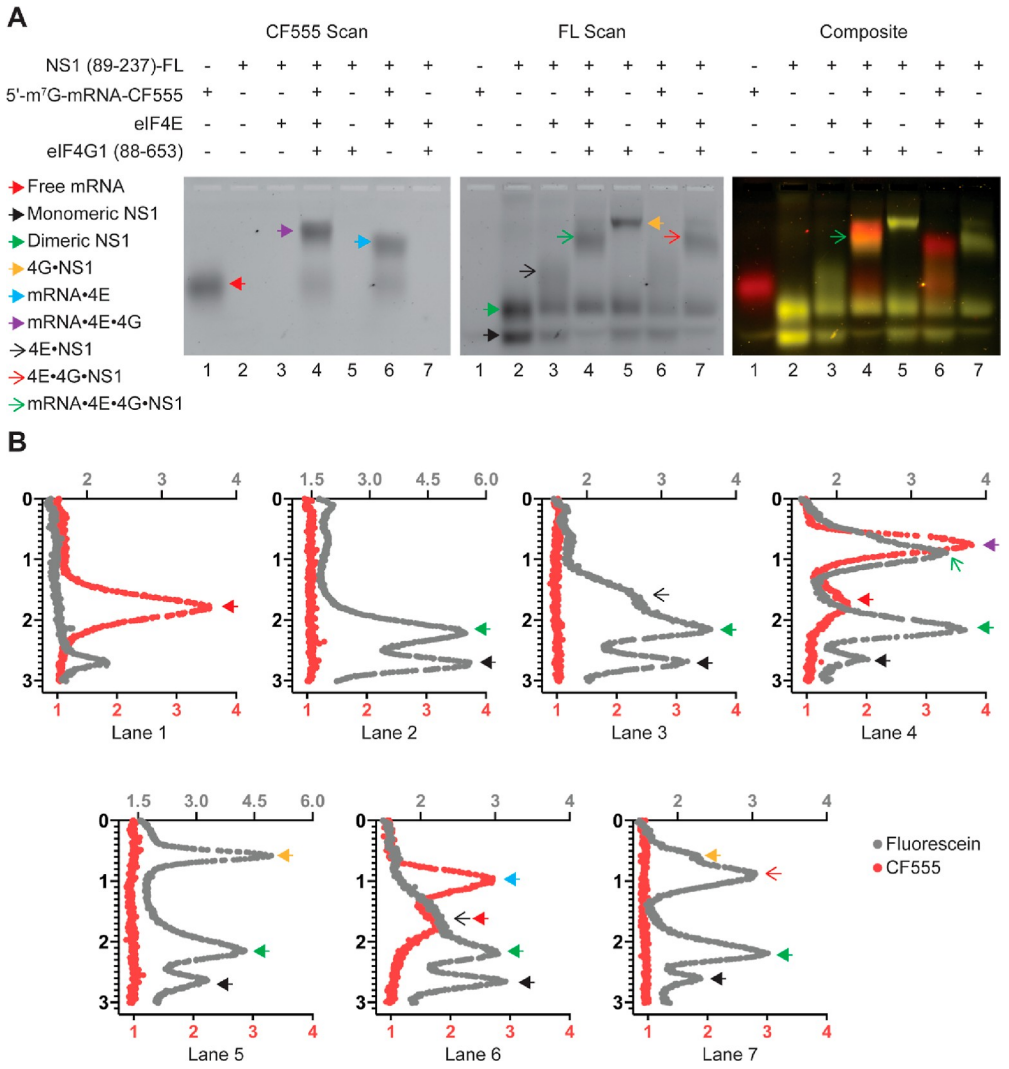

Figure 4. NS1 (89−237) binds to the 5′-m^{7}G-mRNA·eIF4E·eIF4G1 (88−653) complex. (A) Representative EMSA showing the formation of the 5′-m^{7}G-mRNA-CF555·eIF4E·eIF4G1 (88−653) complex and sub-complexes. Left panel, complexes detected by scanning for the CF555 fluorescence emission; middle panel, complexes detected by scanning for the fluorescein emission; right panel, an overlay of both scans with the CF555 emission shown in red and the fluorescein emission shown in yellow. The colored arrowheads indicate each designated complex or unbound fluorophore-labeled protein or mRNA. The plus and minus signs indicate the presence and absence of the indicated biomolecule. (B) ImageJ plot profiles for each fluorophore from each lane of the above EMSA gel. The top horizontal axis corresponds to the intensity (arbitrary units) measured from the fluorescein scan (gray), while the bottom horizontal axis corresponds to the intensity (arbitrary units) measured from the CF555 scan (red). The vertical axis denotes the distance measured from the top to the bottom of the lane (in centimeters). The colored arrowheads indicate the corresponding intensity peak of each designated complex or unbound fluorophore-labeled protein or mRNA.

lower compared to the K_D = 177 nM we report for the NS1 and eIF4E interaction).[31]

We wanted to investigate whether NS1 can bind to the 5′-m^{7}G-mRNA·eIF4E·eIF4G1 complex, as we have shown that it can bind the protein constituents simultaneously and independently. To independently track both the formation of the 5′-m^{7}G-mRNA·eIF4E·eIF4G1 complex and the location of NS1, we used two non-interacting biomolecules, each labeled with a different fluorophore: fluorescein-labeled NS1 (89−237) and CF555 labeled 5′-m^{7}G-mRNA (Figure 3A). As expected, in the absence of NS1 (89−237)-FL, we observed the formation of the 5′-m^{7}G-mRNA·eIF4E·eIF4G1 complex by scanning for CF555 emission (Figure 3B left panel, lane 5). In the presence of NS1 (89−237)-FL, we observed a band that migrated to the same position as the 5′-m^{7}G-mRNA·eIF4E·eIF4G1 complex by scanning for CF555 emission. However, when we examined the position of NS1 (89−237)-FL by scanning for FL emission, we observed that NS1 is present predominantly in a band that runs slightly below the band corresponding to the 5′-m^{7}G-mRNA·eIF4E·eIF4G1 complex (Figure 3B middle panel, lane 6). This can be more clearly visualized when the CF555 emission (red color) and FL emission (yellow color) are superimposed (Figure 3B right panel, lane 6 shows an orange band below the red band formed by the 5′-m^{7}G-mRNA·eIF4E·eIF4G1 complex). The 5′-m^{7}G-mRNA·eIF4E·eIF4G1·NS1 complex migrated faster than the 5′-m^{7}G-mRNA·eIF4E·eIF4G1 complex, suggesting that the NS1-containing complex is more compact and/or more negatively charged. Most likely, NS1 can bind to the 5′-m^{7}G-mRNA·eIF4E·eIF4G1 complex via the interaction with eIF4G1.

Following our initial results showing that the 5′-m^{7}G-mRNA·eIF4E·eIF4G1·NS1 complex can be formed, we wanted to further analyze this complex in the context of other known

https://doi.org/10.1021/acs.biochem.2c00019
Biochemistry 2022, 61, 1485−1494

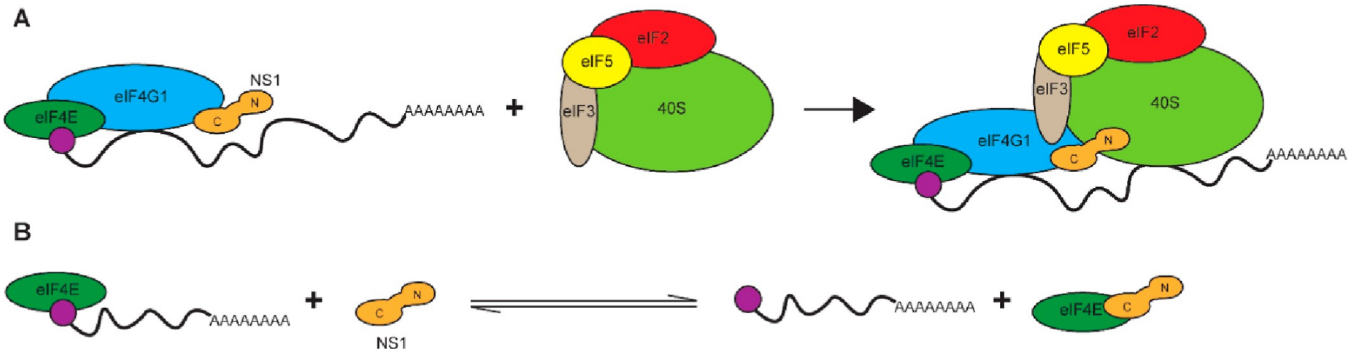

Figure 5. Models for translation regulation by NS1. (A) Interaction of NS1 with the 5′-m^{7}G-mRNA·eIF4E·eIF4G1 complex and the 43S pre-initiation complex. Previous studies have shown that the first 70 amino acids on the N-terminal end of NS1 interact with the 40S subunit.[32] Here, we demonstrate that the last 149 amino acids of the C-terminal end of the NS1 associate with the 5′-m^{7}G-mRNA●eIF4E●eIF4G1 complex. Therefore, NS1 may stimulate translation by stabilizing the interaction of the 5′-m^{7}G-mRNA·eIF4E·eIF4G1 complex with the 43S pre-initiation complex. (B) NS1 binds to eIF4E in the absence of the 5′-m^{7}G-mRNA, which may affect cap-dependent translation.

complexes to verify our results. We performed another EMSA where we formed the 5′-m^{7}G-mRNA·eIF4E·eIF4G1 complex in addition to forming all individual binding complexes of NS1 to compare the multiple band patterns (Figure 4A). Our results indicate that the band pattern for the 5′-m^{7}G-mRNA·eIF4E·eIF4G1·NS1 complex (Figure 4A, middle panel, lane 4) and the band pattern for the eIF4E·eIF4G1·NS1 complex (Figure 4A, middle panel, lane 7) are indistinguishable. However, lane 4 maintained the orange hue, signifying the presence of both NS1 (89−237)-FL (Figure 4A, right panel, yellow color) and the 5′-m^{7}G-mRNA-CF555·eIF4E·eIF4G1 complex (Figure 4A, right panel, red color). Using ImageJ, we plotted the intensity distribution of both the CF-555 dye (red) and fluorescein dye (gray) in each corresponding lane (Figure 4B). We found that the CF-555 intensity peak corresponding to the 5′-m^{7}G-mRNA-containing complex (Lane 4 plot, red) overlaps considerably with the fluorescein intensity peak corresponding to the NS1-containing complex (Lane 4 plot, gray), signifying that NS1 is a constituent of the 5′-m^{7}G-mRNA·eIF4E·eIF4G1 complex. These results are consistent with the fact that eIF4E binds with high affinity to 5′-m^{7}G-mRNA in the presence of eIF4G1 and that NS1 can bind directly to eIF4G1.[18] Thus, NS1 can interact with the translation initiation complex assembled at the 5′-end of mRNAs by binding to eIF4G1. The C-terminal interactions of NS1 with eIF4G1 paired with the N-terminal interactions of NS1 with ribosomes may help explain the previously reported stimulation of translation by NS1.[32,33]

■ DISCUSSION

eIF4G1 is an essential component of the eIF4F complex. During cap-dependent translation initiation, eIF4G1 interacts with eIF4E, eIF4A, poly-A binding Protein 1 (PABP1), and other initiation factors to recruit the 40S ribosomal subunit and begin translation.[27] Considering the importance of eIF4G1's role in translation, it would stand to reason that IAV would also target eIF4G1 as other viruses, such as Zika Virus and HIV-1, have been shown to target this protein as a means to influence host translation.[34,35] The fundamental need for eIF4G1 in IAV translation was confirmed by a previous study demonstrating that a decrease of functional eIF4G1 leads to a corresponding decline of translated IAV proteins.[36] Though the reason for NS1 binding to eIF4G1 is unclear, we further characterized this interaction by providing visual evidence of this protein−protein complex and determining the K_D value for this interaction.

Much like eIF4G1, eIF4E is crucial in forming the eIF4F complex as it binds the 5′-m^{7}G cap structure and aids in directing ribosomes to mRNAs for translation.[37] This cap-binding protein is heavily regulated by endogenous pathways to modulate cap-dependent translation and, as such, is the limiting factor for the eIF4F complex.[37,38] The direct correlation of eIF4E with cap-dependent translation is best seen in cancer where eIF4E is often overexpressed, leading to tumor formation.[39,40] Previous studies have shown that during IAV infection, eIF4E is excessively dephosphorylated, leading to inactivation.[30] Although the mechanism is still unclear, the IAV does not require a functional eIF4E to translate a viral protein successfully.[28] These findings, combined with our results, indicate that NS1 may target eIF4E in an antagonistic manner. It is possible that NS1 specifically inhibits eIF4E-dependent translation, while cap-dependent but eIF4E-independent translation is stimulated to support infection.[41−44] Additionally, IAV mRNAs may be translated without the formation of the mRNA closed-loop structure when the activity of eIF4E is inhibited by NS1.[45,46] More studies are needed to understand the functional significance of NS1 binding to eIF4E.

The NS1 protein is highly overexpressed during infection, and it is responsible for an ample number of viral processes that antagonize the host immune response and assist in the proliferation of the IAV.[8,9] In addition to facilitating the circumvention of the host immune response, NS1 has also been shown to increase mRNA translation.[32,33,47] Though it is uncertain how NS1 increases translation, in this report, we expand the theory of NS1 acting as a translation initiation stimulator. First, the binding site of NS1 on eIF4G1 does not overlap with any other known binding sites on eIF4G1, suggesting that NS1 can bind the eIF4E·eIF4G1 complex, while eIF4G1 is bound to other initiation factors.[16,27] Second, only the C-terminal end of NS1 is required to bind the eIF4E·eIF4G1 complex, indicating that the NS1 RBD remains available for interactions with other biomolecules. Third, previous studies have shown that the NS1 RBD stimulates translation by promoting the association of the ribosomes with mRNAs.[32] Fourth, the NS1 RBD can interact with PABP1 without the C-terminal region of NS1.[20,48,49] With our results paired with the data mentioned above, we theorize that NS1 may form a network of interactions with eIF4G1, PABP1, and

https://doi.org/10.1021/acs.biochem.2c00019
Biochemistry 2022, 61, 1485−1494

the 43S pre-initiation complex to stimulate translation (Figure 5).

■ ASSOCIATED CONTENT

Supporting Information

The Supporting Information is available free of charge at https://pubs.acs.org/doi/10.1021/acs.biochem.2c00019.

EMSA of NS1(89−237)-FL and BSA, EMSA of full-length NS1 and NS1 (89−237) addition to 5′-m^{7}G-mRNA-FL·eIF4E complex, EMSA of m^{7}G(5′)ppp(5′)G cap analogue addition to NS1(89-237)-FL·eIF4E complex, EMSA of NS1(89−237)-FL protein−protein complexes following RNAse incubation, EMSA of 5′-m^{7}G-mRNA and protein complexes, and SDS−PAGE of proteins utilized for the experiments (PDF)

Accession Codes

H3N2 NS1: P03495. H5N1 NS1: D2SJD8. eIF4E: P06730. eIF4G1: Q04637.

■ AUTHOR INFORMATION

Corresponding Author

Simpson Joseph − *Department of Chemistry and Biochemistry, University of California at San Diego, La Jolla, California 92093-0314, United States;* orcid.org/0000-0002-0552-8221; Phone: Phone: 858-822-2957; Email: sjoseph@ucsd.edu

Author

Alejandro Cruz − *Department of Chemistry and Biochemistry, University of California at San Diego, La Jolla, California 92093-0314, United States*

Complete contact information is available at: https://pubs.acs.org/10.1021/acs.biochem.2c00019

Author Contributions

All authors designed the experiments. A.C. performed the experiments, and all authors discussed the results. A.C. wrote the paper with input from S.J. S.J. supervised all aspects of the work.

Funding

This work was supported by the National Institutes of Health (R01GM114261 and R35GM141864 to S.J.)

Notes

The authors declare no competing financial interest.

The data that support the findings of this study are available from the corresponding author on reasonable request.

■ ACKNOWLEDGMENTS

We thank Cyrus de Rozières and Alberto Pequeno for the NS1, eIF4E, and eIF4G1 constructs and technical support during the early stages of the project.

■ REFERENCES

(1) Rolfes, M. A.; Foppa, I. M.; Garg, S.; Flannery, B.; Brammer, L.; Singleton, J. A.; Burns, E.; Jernigan, D.; Olsen, S. J.; Bresee, J.; Reed, C. Annual Estimates of the Burden of Seasonal Influenza in the United States: A Tool for Strengthening Influenza Surveillance and Preparedness. *Influenza Other Respir. Viruses* **2018**, *12*, 132−137.

(2) Molinari, N.-A. M.; Ortega-Sanchez, I. R.; Messonnier, M. L.; Thompson, W. W.; Wortley, P. M.; Weintraub, E.; Bridges, C. B. The Annual Impact of Seasonal Influenza in the US: Measuring Disease Burden and Costs. *Vaccine* **2007**, *25*, 5086−5096.

(3) Taubenberger, J. K.; Morens, D. M. The Pathology of Influenza Virus Infections. *Annu. Rev. Pathol.* **2008**, *3*, 499.

(4) Webster, R. G.; Bean, W. J.; Gorman, O. T.; Chambers, T. M.; Kawaoka, Y. Evolution and Ecology of Influenza A Viruses. *Microbiol. Mol. Biol. Rev.* **1992**, *56*, 152−179.

(5) Paterson, D.; Fodor, E. Emerging Roles for the Influenza A Virus Nuclear Export Protein (NEP). *PLoS Pathog.* **2012**, *8*, No. e1003019.

(6) Inglis, S. C.; Barrett, T.; Brown, C. M.; Almond, J. W. The Smallest Genome RNA Segment of Influenza Virus Contains Two Genes That May Overlap. *Proc. Natl. Acad. Sci. U.S.A.* **1979**, *76*, 3790−3794.

(7) Wise, H. M.; Foeglein, A.; Sun, J.; Dalton, R. M.; Patel, S.; Howard, W.; Anderson, E. C.; Barclay, W. S.; Digard, P. A Complicated Message: Identification of a Novel PB1-Related Protein Translated from Influenza A Virus Segment 2 MRNA. *J. Virol.* **2009**, *83*, 8021−8031.

(8) Hale, B. G.; Randall, R. E.; Ortín, J.; Jackson, D. The Multifunctional NS1 Protein of Influenza A Viruses. *J. Gen. Virol.* **2008**, *89*, 2359−2376.

(9) Ji, Z.-x.; Wang, X.-q.; Liu, X.-f. NS1: A Key Protein in the "Game" Between Influenza A Virus and Host in Innate Immunity. *Front. Cell. Infect. Microbiol.* **2021**, *11*, 670177.

(10) Carrillo, B.; Choi, J.-M.; Bornholdt, Z. A.; Sankaran, B.; Rice, A. P.; Prasad, B. V. V. The Influenza A Virus Protein NS1 Displays Structural Polymorphism. *J. Virol.* **2014**, *88*, 4113−4122.

(11) Hale, B. G. Conformational Plasticity of the Influenza A Virus NS1 Protein. *J. Gen. Virol.* **2014**, *95*, 2099−2105.

(12) Han, C. W.; Jeong, M. S.; Jang, S. B. Structure and Function of the Influenza. *J. Microbiol. Biotechnol.* **2019**, *29*, 1184−1192.

(13) Merrick, W. C.; Pavitt, G. D. Protein Synthesis Initiation in Eukaryotic Cells. *Cold Spring Harbor Perspect. Biol.* **2018**, *10*, a033092.

(14) Parsyan, A.; Svitkin, Y.; Shahbazian, D.; Gkogkas, C.; Lasko, P.; Merrick, W. C.; Sonenberg, N. MRNA Helicases: The Tacticians of Translational Control. *Nat. Rev. Mol. Cell Biol.* **2011**, *12*, 235−245.

(15) Shirokikh, N. E.; Preiss, T. Translation Initiation by Cap-Dependent Ribosome Recruitment: Recent Insights and Open Questions. *WIREs RNA* **2018**, *9*, No. e1473.

(16) Aragón, T.; Luna, S.; de la Luna, I.; Carrasco, L.; Ortín, J.; Nieto, A. Eukaryotic Translation Initiation Factor 4GI Is a Cellular Target for NS1 Protein, a Translational Activator of Influenza Virus. *Mol. Cell. Biol.* **2000**, *20*, 6259−6268.

(17) Grüner, S.; Peter, D.; Weber, R.; Wohlbold, L.; Chung, M.-Y.; Weichenrieder, O.; Valkov, E.; Igreja, C.; Izaurralde, E. The Structures of EIF4E-EIF4G Complexes Reveal an Extended Interface to Regulate Translation Initiation. *Mol. Cell* **2016**, *64*, 467−479.

(18) Friedland, D. E.; Wooten, W. N. B.; LaVoy, J. E.; Hagedorn, C. H.; Goss, D. J. A Mutant of Eukaryotic Protein Synthesis Initiation Factor EIF4EK119A Has an Increased Binding Affinity for Both M7G Cap Analogues and EIF4G Peptides. *Biochemistry* **2005**, *44*, 4546−4550.

(19) Weeks, S. D.; Drinker, M.; Loll, P. J. Ligation Independent Cloning Vectors for Expression of SUMO Fusions. *Protein Expr. Purif.* **2007**, *53*, 40−50.

(20) de Rozières, C. M.; Joseph, S. Influenza A Virus NS1 Protein Binds as a Dimer to RNA-Free PABP1 but Not to the PABP1·Poly(A) RNA Complex. *Biochemistry* **2020**, *59*, 4439−4448.

(21) Fuchs, A.-L.; Neu, A.; Sprangers, R. A General Method for Rapid and Cost-Efficient Large-Scale Production of 5′ Capped RNA. *RNA* **2016**, *22*, 1454−1466.

(22) Park, S.-H.; Raines, R. T. Fluorescence Gel Retardation Assay to Detect Protein-Protein Interactions. In *Protein-Protein Interactions: Methods and Applications*; Fu, H., Ed.; Methods in Molecular Biology; Humana Press: Totowa, NJ, 2004; pp 155−159.

(23) Wagstaff, K. M.; Dias, M. M.; Alvisi, G.; Jans, D. A. Quantitative Analysis of Protein-Protein Interactions by Native Page/Fluorimaging. *J. Fluoresc.* **2005**, *15*, 469−473.

(24) Athar, Y. M.; Joseph, S. RNA-Binding Specificity of the Human Fragile X Mental Retardation Protein. *J. Mol. Biol.* **2020**, *432*, 3851−3868.

(25) Aramini, J. M.; Hamilton, K.; Ma, L.-C.; Swapna, G. V. T.; Leonard, P. G.; Ladbury, J. E.; Krug, R. M.; Montelione, G. T. 19F NMR Reveals Multiple Conformations at the Dimer Interface of the Nonstructural Protein 1 Effector Domain from Influenza A Virus. *Structure* **2014**, *22*, 515−525.
(26) Aramini, J. M.; Ma, L.-C.; Zhou, L.; Schauder, C. M.; Hamilton, K.; Amer, B. R.; Mack, T. R.; Lee, H.-W.; Ciccosanti, C. T.; Zhao, L.; Xiao, R.; Krug, R. M.; Montelione, G. T. Dimer Interface of the Effector Domain of Non-Structural Protein 1 from Influenza A Virus. *J. Biol. Chem.* **2011**, *286*, 26050−26060.
(27) Prévôt, D.; Darlix, J.-L.; Ohlmann, T. Conducting the Initiation of Protein Synthesis: The Role of EIF4G. *Biol. Cell.* **2003**, *95*, 141−156.
(28) Burgui, I.; Yángüez, E.; Sonenberg, N.; Nieto, A. Influenza Virus MRNA Translation Revisited: Is the EIF4E Cap-Binding Factor Required for Viral MRNA Translation? *J. Virol.* **2007**, *81*, 12427−12438.
(29) Bier, K.; York, A.; Fodor, E. Cellular Cap-Binding Proteins Associate with Influenza Virus MRNAs. *J. Gen. Virol.* **2011**, *92*, 1627−1634.
(30) Feigenblum, D.; Schneider, R. J. Modification of Eukaryotic Initiation Factor 4F during Infection by Influenza Virus. *J. Virol.* **1993**, *67*, 3027−3035.
(31) Wojtczak, A.; Kasprzyk, R.; Warmiński, M.; Ubych, K.; Kubacka, D.; Sikorski, P. J.; Jemielity, J.; Kowalska, J. Evaluation of Carboxyfluorescein-Labeled 7-Methylguanine Nucleotides as Probes for Studying Cap-Binding Proteins by Fluorescence Anisotropy. *Sci. Rep.* **2021**, *11*, 7687.
(32) Panthu, B.; Terrier, O.; Carron, C.; Traversier, A.; Corbin, A.; Balvay, L.; Lina, B.; Rosa-Calatrava, M.; Ohlmann, T. The NS1 Protein from Influenza Virus Stimulates Translation Initiation by Enhancing Ribosome Recruitment to MRNAs. *J. Mol. Biol.* **2017**, *429*, 3334−3352.
(33) Liu, Y.; Chin, J. M.; Choo, E. L.; Phua, K. K. L. Messenger RNA Translation Enhancement by Immune Evasion Proteins: A Comparative Study between EKB (Vaccinia Virus) and NS1 (Influenza A Virus). *Sci. Rep.* **2019**, *9*, 11972.
(34) Hill, M. E.; Kumar, A.; Wells, J. A.; Hobman, T. C.; Julien, O.; Hardy, J. A. The Unique Cofactor Region of Zika Virus NS2B−NS3 Protease Facilitates Cleavage of Key Host Proteins. *ACS Chem. Biol.* **2018**, *13*, 2398−2405.
(35) Castelló, A.; Franco, D.; Moral-López, P.; Berlanga, J. J.; Álvarez, E.; Wimmer, E.; Carrasco, L. HIV- 1 Protease Inhibits Cap- and Poly(A)-Dependent Translation upon EIF4GI and PABP Cleavage. *PLoS One* **2009**, *4*, No. e7997.
(36) Yángüez, E.; Castello, A.; Welnowska, E.; Carrasco, L.; Goodfellow, I.; Nieto, A. Functional Impairment of EIF4A and EIF4G Factors Correlates with Inhibition of Influenza Virus MRNA Translation. *Virology* **2011**, *413*, 93−102.
(37) Batool, A.; Aashaq, S.; Andrabi, K. I. Eukaryotic Initiation Factor 4E (EIF4E): A Recap of the Cap-binding Protein. *J. Cell. Biochem.* **2019**, *120*, 14201−14212.
(38) Rhoads, R. E. EIF4E: New Family Members, New Binding Partners, New Roles. *J. Biol. Chem.* **2009**, *284*, 16711−16715.
(39) Wendel, H.-G.; Silva, R. L. A.; Malina, A.; Mills, J. R.; Zhu, H.; Ueda, T.; Watanabe-Fukunaga, R.; Fukunaga, R.; Teruya-Feldstein, J.; Pelletier, J.; Lowe, S. W. Dissecting EIF4E Action in Tumorigenesis. *Genes Dev.* **2007**, *21*, 3232.
(40) Carroll, M.; Borden, K. L. B. The Oncogene EIF4E: Using Biochemical Insights to Target Cancer. *J. Interferon Cytokine Res.* **2013**, *33*, 227−238.
(41) Borden, K. L. B.; Volpon, L. The Diversity, Plasticity, and Adaptability of Cap-Dependent Translation Initiation and the Associated Machinery. *RNA Biol.* **2020**, *17*, 1239−1251.
(42) de la Parra, C.; Ernlund, A.; Alard, A.; Ruggles, K.; Ueberheide, B.; Schneider, R. J. A Widespread Alternate Form of Cap-Dependent MRNA Translation Initiation. *Nat. Commun.* **2018**, *9*, 3068.
(43) Lee, A. S. Y.; Kranzusch, P. J.; Doudna, J. A.; Cate, J. H. D. EIF3d Is an MRNA Cap-Binding Protein That Is Required for Specialized Translation Initiation. *Nature* **2016**, *536*, 96−99.
(44) de Rozières, C. M.; Pequeno, A.; Shahabi, S.; Lucas, T. M.; Godula, K.; Ghosh, G.; Joseph, S. PABP1 Drives the Selective Translation of Influenza A Virus MRNA. *J. Mol. Biol.* **2022**, *434*, 167460.
(45) Adivarahan, S.; Livingston, N.; Nicholson, B.; Rahman, S.; Wu, B.; Rissland, O. S.; Zenklusen, D. Spatial Organization of Single MRNPs at Different Stages of the Gene Expression Pathway. *Mol. Cell* **2018**, *72*, 727−738.
(46) Vicens, Q.; Kieft, J. S.; Rissland, O. S. Revisiting the Closed-Loop Model and the Nature of MRNA 5'-3' Communication. *Mol. Cell* **2018**, *72*, 805−812.
(47) Liu, Y.; Chia, Z. H.; Liew, J. N. M. H.; Or, S. M.; Phua, K. K. L. Modulation of MRNA Translation and Cell Viability by Influenza A Virus Derived Nonstructural Protein 1. *Nucleic Acid Therapeut.* **2018**, *28*, 200−208.
(48) Burgui, I.; Aragón, T.; Ortín, J.; Nieto, A. PABP1 and EIF4GI Associate with Influenza Virus NS1 Protein in Viral MRNA Translation Initiation Complexes. *J. Gen. Virol.* **2003**, *84*, 3263−3274.
(49) Arias-Mireles, B. H.; de Rozieres, C. M.; Ly, K.; Joseph, S. RNA Modulates the Interaction between Influenza A Virus NS1 and Human PABP1. *Biochemistry* **2018**, *57*, 3590−3598.

https://doi.org/10.1021/acs.biochem.2c00019
Biochemistry 2022, 61, 1485−1494